Implementation of a frequency-domain neutron noise analysis method in a production-level continuous energy Monte Carlo code: Verification and application in a BWR

Yamamoto, Toshihiro

Elsevier Editorial System(tm) for Annals of Nuclear Energy

Manuscript Draft

Manuscript Number: ANUCENE-D-17-00933R1

Title: Implementation of a frequency-domain neutron noise analysis method in a production-level continuous energy Monte Carlo code: Verification and application in a BWR

Article Type: Full Length Article

Keywords: Monte Carlo; neutron noise; frequency domain; BWR

Corresponding Author: Dr. Toshihiro Yamamoto, Ph.D

Corresponding Author's Institution: Kyoto University

First Author: Toshihiro Yamamoto, Ph.D

Order of Authors: Toshihiro Yamamoto, Ph.D

Abstract: A Monte Carlo algorithm for solving the transport equation of the neutron noise in the frequency domain has been newly implemented into a production-level continuous energy Monte Carlo code, MCNP. Using the continuous energy Monte Carlo code, accurate neutron noise calculations can be performed with fewer approximations. The implemented algorithm is based on a method that was previously developed by the author of this paper. The modified code is currently applicable to neutron noise calculations only within the plateau frequency range. The modified code is applied to the neutron noise calculations in a one-dimensional homogeneous multiplying system to verify its effectiveness through comparison with a two-energy group in-house research-purpose code. The neutron noise calculations for a benchmark model of a BWR core are performed using the modified MCNP code. The spatial and frequency characteristics of the neutron noise propagation in the BWR core are investigated through the calculations. The neutron noise near the noise source differs largely from the point kinetics because of the higher order mode effect.

KYOTO UNIVERSITY
RESEARCH REACTOR INSTITUTE
Kumatori-cho, Sennan-gun, OSAKA, JAPAN

Research Reactor Institute
Kyoto University
Kumatori-cho, Sennan-gun,
Osaka, 590-0494 JAPAN
Phone 81-72-451-2414
Fax 81-72-451-2658

31 January, 2018

Prof. S Mostafa Ghiaasiaan
Editor of Annals of Nuclear Energy

Dear Prof. Ghiaasiaan:

I am submitting a revised manuscript, ANUCENE-D-17-00933, entitled

> Implementation of a frequency-domain neutron noise analysis method in a production-level continuous energy Monte Carlo code: Verification and application in a BWR

to *Annals of Nuclear Energy*.

Sincerely yours
Toshihiro Yamamoto

Implementation of a frequency-domain neutron noise analysis method in a production-level continuous energy Monte Carlo code: Verification and application in a BWR

Toshihiro Yamamoto*

Research Reactor Institute, Kyoto University, 2 Asashiro Nishi, Kumatori-cho, Sennan-gun, Osaka, 590-0494, Japan

Abstract

A Monte Carlo algorithm for solving the transport equation of the neutron noise in the frequency domain has been newly implemented into a production-level continuous energy Monte Carlo code, MCNP. Using the continuous energy Monte Carlo code, accurate neutron noise calculations can be performed with fewer approximations. The implemented algorithm is based on a method that was previously developed by the author of this paper. The modified code is currently applicable to neutron noise calculations only within the plateau frequency range. The modified code is applied to the neutron noise calculations in a one-dimensional homogeneous multiplying system to verify its effectiveness through comparison with a two-energy group in-house research-purpose code. The neutron noise calculations for a benchmark model of a BWR core are performed using the modified MCNP code. The spatial and frequency characteristics of the neutron noise propagation in the BWR core are investigated

* Corresponding author. Tel:+81 72 451 2414; fax:+81 72 451 2658
E-mail address: toshihiro.yamamoto223@gmail.com (T.Yamamoto)

through the calculations. The neutron noise near the noise source differs largely from the point kinetics because of the higher order mode effect.

Keywords: Monte Carlo; neutron noise; frequency domain; BWR.

1. Introduction

Measuring neutron noise (i.e., the difference between a time-varying neutron flux and its steady state value) in a reactor core is an effective means for core monitoring or diagnoses, such as an unseated fuel assembly, abnormal vibrations of the internal core structures, or flow blockage (Jonsson et al., 2012; Viebach et al., 2017). Research activities on the core monitoring technique are being pursued by many institutions. Recently, the CORTEX project, a research and innovation action aiming at developing an innovative core monitoring technique using the fluctuations in neutron flux, started in the Euratom 2016-2017 work program (Demazière et al., 2017). The reconstruction or unfolding of the noise source is an important process to identify the anomalies occurring within the reactor core. Various reconstruction or unfolding techniques have been developed to date (Glöckler and Pázsit, 1987; Demazière and Andhill, 2005; Hosseini and Vosoughi, 2013; Hosseini and Vosoughi, 2014). Regardless of the technique used for the reconstruction or unfolding process, the calculation of the neutron noise at the detector positions caused by an anticipated noise source is required to solve an inversion problem to identify the anomalies in a core. The response of the neutron noise induced by a noise source can be calculated by an analytical formula (Behringer et al., 1977; Pázsit and Analytis, 1980; Jonsson et al., 2012) or by solving the neutron noise diffusion or transport equation in the frequency domain. Thus, developing a noise calculation method with high accuracy is an important task towards enhancing nuclear safety through the use of reactor noise diagnostics.

A variety of calculation tools for obtaining the neutron noise responses have been developed thus far; they are mostly based on diffusion theory (Demazière, 2004; Demazière and Pázsit, 2009; Pázsit and Demazière, 2010; Larsson et al., 2011; Demazière, C., 2011; Larsson and Demazière, 2012a; Larsson and Demazière, 2012b; Hosseini and Vosoughi, 2012). The extension of the noise calculation to transport theory was attempted by (Yamamoto, 2013) and (Rouchon et al., 2017). In these studies involving transport theory, the neutron noise transport equation was solved using the Monte Carlo method. In (Yamamoto, 2013), the neutron noise distributions were calculated both using diffusion theory and using the Monte Carlo method. The comparison highlighted the unsatisfactory results of diffusion theory, particularly near the noise source position, suggesting the necessity of introducing the transport method for neutron noise calculations. Unlike the diffusion equation for neutron noise, which can be solved using the conventional numerical techniques, the Monte Carlo method is confronted with some difficulties, especially for low- and high-frequency noise. If a conventional Monte Carlo algorithm (i.e., implicit capture and Russian roulette, etc.) is employed, a very large number of particles having positive or negative weights are produced for low- and high-frequency noise, resulting in abnormal termination of the computation. The positive and negative weights need to be canceled to prevent the exploding number of particles, but a special technique must be introduced for the cancellation because no two particles exist at the same position. In contrast, the difficulty of the exploding number of particles does not occur for the plateau frequency range (Rouchon et al., 2017), which is approximately between 0.01 Hz ($\approx\lambda/(2\pi)$) and 40 Hz ($\approx(\lambda + \beta/\Lambda)/(2\pi)$) for light water reactors. To circumvent this difficulty that occurs outside the plateau frequency region, Yamamoto (2013) and Yamamoto and Sakamoto (2015) introduced a weight cancellation technique and a power iteration-like algorithm.

However, the countermeasures for managing the exploding number of particles demand that the whole calculation domain should be discretized into many small subdomains, where positive and negative particle weights are cancelled. Installing the weight cancellation technique into a production-level Monte Carlo code would cause the code to be less versatile. Thus, the numerical application in (Yamamoto, 2013) was limited to a homogeneous simple geometry that was modeled using an in-house research-purpose code. Rouchon et al. (2017) developed a new Monte Carlo method that does not require the weight cancellation technique. The new method removes the implicit capture technique and adds a pseudo total cross section to the neutron noise equation.

The advantage of introducing the continuous energy Monte Carlo method for neutron noise calculations is that the Monte Carlo method can model the three-dimensional fine structures in a power reactor core without spatial homogenization and it is free from the inaccuracy involved in energy group collapsing. The implementation of the frequency domain Monte Carlo method into a production-level continuous energy Monte Carlo code is important in terms of expanding the availability of the method. Remarkable improvement in the accuracy of the neutron noise calculation can be expected by using the continuous energy Monte Carlo code. Neutron noise Monte Carlo calculations in the frequency domain have thus far been performed using an in-house research-purpose code. Thus, to expand the implementation of the Monte Carlo method in neutron noise calculations, in this paper, the frequency domain Monte Carlo method is implemented into a production-level continuous energy Monte Carlo code, MCNP 4C (Briesmeister, 2000). The Monte Carlo technique adopted in this paper is based on the previously developed complex-valued weight Monte Carlo method in (Yamamoto, 2012; Yamamoto, 2013). The method used in this paper is available only for the plateau frequency range, where

the number of particles can be controlled without introducing a new method. The implementation of the methods developed in (Rouchon et al., 2017) or some other useful techniques will be left as a future work.

As the first step, the verification of the modified MCNP code is performed by comparing the code with the in-house research-purpose Monte Carlo code (Yamamoto, 2013) for a very simple multiplying system. Next, neutron noise transport calculations are performed for a BWR benchmark model. The properties of the noise propagation within the BWR core structure are discussed.

2. Neutron Noise Equation in the Transport Theory

The fundamental theory on the propagation of neutron noise in the frequency domain has been presented in previously published literature reports. Within the diffusion approximation, the neutron noise propagation has been discussed in many publications (Behringer et al., 1977; Behringer et al., 1979; Demazière, 2004; Demazière and Pázsit, 2009; Larsson et al., 2011; Demazière, C., 2011; Larsson and Demazière, 2012a; Larsson and Demazière, 2012b). Transport theory has been recently introduced in some papers (Yamamoto, 2013; Yamamoto and Sakamoto, 2015; Rouchon et al., 2017). In this section, the transport equation to be solved for neutron noise propagation in a reactor core is only briefly explained.

The neutron noise in the time domain is defined by

$$\delta\phi(\mathbf{r},\mathbf{\Omega},E,t) \equiv \phi(\mathbf{r},\mathbf{\Omega},E,t) - \phi_0(\mathbf{r},\mathbf{\Omega},E)\,, \tag{1}$$

where $\phi(\mathbf{r},\mathbf{\Omega},E,t)$ = the neutron flux at position $\mathbf{r}$ with energy E and direction $\mathbf{\Omega}$ at time t, and the subscript "0" denotes the mean value. The neutron noise is induced by the fluctuation of the macroscopic cross sections around their mean value:

$$\delta\Sigma_x(\mathbf{r},E,t) \equiv \Sigma_x(\mathbf{r},E,t) - \Sigma_{x0}(\mathbf{r},E)\,, \tag{2}$$

where x = t, s, or f. The neutron noise in the frequency domain is obtained by Fourier transforming the neutron noise in the time domain:

$$\delta\phi(\mathbf{r},\mathbf{\Omega},E,\omega) \equiv \int_{-\infty}^{+\infty} \delta\phi(\mathbf{r},\mathbf{\Omega},E,t)e^{-i\omega t}dt\,, \tag{3}$$

where ω = the angular frequency and $i = \sqrt{-1}$. The neutron noise transport equation in the frequency domain is derived from the time-dependent neutron transport equation and the equation for the delayed neutron precursor density using a linear approximation and a Fourier transformation. The equation finally obtained is shown below:

$$\begin{aligned}
&\mathbf{\Omega}\cdot\nabla\delta\phi(\mathbf{r},\mathbf{\Omega},E,\omega) + \Sigma_{t0}(\mathbf{r},E)\delta\phi(\mathbf{r},\mathbf{\Omega},E,\omega)\\
&= \int_{4\pi} d\mathbf{\Omega}' \int dE' \Sigma_{s0}(\mathbf{r},\mathbf{\Omega}'\to\mathbf{\Omega},E'\to E)\delta\phi(\mathbf{r},\mathbf{\Omega}',E',\omega)\\
&+ \frac{\chi(E)}{4\pi k_{eff}}\left(1-\frac{i\omega\beta}{i\omega+\lambda}\right)\int_{4\pi} d\mathbf{\Omega}' \int dE' \nu\Sigma_{f0}(\mathbf{r},E')\delta\phi(\mathbf{r},\mathbf{\Omega}',E',\omega)\\
&- \frac{i\omega}{\upsilon(E)}\delta\phi(\mathbf{r},\mathbf{\Omega},E,\omega) + S(\mathbf{r},\mathbf{\Omega},E,\omega),
\end{aligned} \tag{4}$$

where Σ_t =the macroscopic total cross section, Σ_s = the macroscopic scattering cross section, Σ_f =the macroscopic fission cross section, χ = the fission neutron spectrum, ν =the number of neutrons per fission, υ = the neutron speed, β = the fraction of the delayed neutrons, λ = the time decay constant of the delayed neutron precursors, and S = the noise source. For simplicity, the fission neutron spectrum of the delayed neutrons is assumed to be the same as that of the prompt neutrons. Furthermore, one delayed neutron group is assumed. The noise source, which is induced by the temporal fluctuations of the macroscopic cross sections, is defined by

$$\begin{aligned}
&S(\mathbf{r},\mathbf{\Omega},E,\omega) \equiv -\delta\Sigma_t(\mathbf{r},E,\omega)\phi_0(\mathbf{r},\mathbf{\Omega},E)\\
&+ \int_{4\pi} d\mathbf{\Omega}' \int dE' \delta\Sigma_s(\mathbf{r},\mathbf{\Omega}'\to\mathbf{\Omega},E'\to E,\omega)\phi_0(\mathbf{r},\mathbf{\Omega}',E')\\
&+ \frac{\chi(E)}{4\pi k_{eff}}\left(1-\frac{i\omega\beta}{i\omega+\lambda}\right)\int_{4\pi} d\mathbf{\Omega}' \int dE' \nu\delta\Sigma_f(\mathbf{r},E',\omega)\phi_0(\mathbf{r},\mathbf{\Omega}',E')
\end{aligned} \tag{5}$$

where $\delta\Sigma_x(\mathbf{r},E,\omega)$ is the Fourier transform of the fluctuation of the reaction x:

$$\delta\Sigma_x(\mathbf{r},E,\omega) \equiv \int_{-\infty}^{+\infty} \delta\Sigma_x(\mathbf{r},E,t)e^{-i\omega t}dt\,. \tag{6}$$

In most cases, our interest is focused on a neutron noise propagation in a critical state reactor core. Thus, the neutron production terms in Eqs. (4) and (5) are divided by k_{eff} to eliminate the bias in the calculated k_{eff} that usually deviates from unity.

Eq. (4) is the transport equation to be solved for the neutron noise propagation in a critical state reactor core. In the next section, an algorithm to solve this equation using the Monte Carlo method is explained briefly.

3. Monte Carlo Algorithm to Solve the Neutron Noise Equation

Some algorithms for solving the neutron noise transport equation, Eq. (4), have been proposed, e.g., those published in (Yamamoto, 2013; Rouchon et al., 2017). As stated in Sec. 1, a special technique is required to suppress the diverging particle population that stems from fission chain reactions in a frequency domain neutron noise propagation. The abovementioned two papers present different proposed methods for suppressing the divergence. However, it is known that the divergence does not emerge for the plateau frequency range that extends approximately between λ and $\lambda + \beta/\Lambda$, where Λ = the prompt neutron generation time. Implementing the algorithm for avoiding the problem of divergence into a production-level Monte Carlo code may require an enormous number of modifications. In this paper, an algorithm for solving the neutron noise transport equation, Eq. (4), which is valid for the plateau region only, is implemented into a production-level Monte Carlo code, MCNP (Briesmeister, 2000). In other words, the modified code, where the algorithm for suppressing the divergence is not implemented, does not have the capability to calculate the neutron noise outside the plateau frequency range.

In this section, the fundamentals to solve the neutron noise transport equation, Eq.

(4), are briefly shown; the approach is based on a previously published paper. The method presented by Yamamoto (2013) is different from that presented by Rouchon et al. (2017). This paper follows the algorithm of Yamamoto (2013).

(1) Transport of particles

First, a particle originates from the site of a noise source. The position, direction, energy, and weight of the particle are determined according to Eq. (5). The weight is generally complex-valued. Determination of the source term is not straightforward and is left to future work because the steady-state neutron flux ϕ_0 must be calculated.

To solve Eq. (4) using the Monte Carlo method, we must take into account the third term on the right-hand side of Eq. (4) during the random walk processes of the Monte Carlo calculation. Several methods are available to accomplish this task (Yamamoto, 2013; Rouchon et al., 2017). The method adopted in this paper is as follows. As the particle flies a distance s_j in the *j*th flight path, the initial weight W_j changes to

$$W_{j+1} = W_j \exp\left(-\frac{i\omega}{\upsilon_j(E)} s_j\right) = W_j\left(\cos\left(\frac{\omega}{\upsilon_j(E)} s_j\right) - i\sin\left(\frac{\omega}{\upsilon_j(E)} s_j\right)\right), \tag{7}$$

where the particle weight W_j is a complex-valued quantity and the real and imaginary parts can be positive and negative. The flight distance s_j is determined by $s_j = -\ell n\xi / \Sigma_t$, where ξ is a uniform pseudo-random number from (0, 1), which is identical to the conventional Monte Carlo algorithm. Eq. (7) indicates that the particle weight changes continuously during the flight path. Thus, after the *j*th flight path over the distance s_j, the track length estimator is described by

$$\begin{aligned} TL_j &= \int_0^{s_j} W_j \exp\left(-\frac{i\omega}{\upsilon_j(E)} s'\right) ds' = W_j \frac{i\upsilon_j(E)}{\omega}\left(\exp\left(-\frac{i\omega}{\upsilon_j(E)} s_j\right) - 1\right) \\ &= W_j \frac{\upsilon_j(E)}{\omega}\left(\sin\left(\frac{\omega}{\upsilon_j(E)} s_j\right) + i\left(\cos\left(\frac{\omega}{\upsilon_j(E)} s_j\right) - 1\right)\right). \end{aligned} \tag{8}$$

(2) Implicit capture and Russian roulette

At each collision, the implicit capture is used as for the conventional Monte Carlo method. A weight W_j before collision changes to

$$W_j' = W_j \frac{\Sigma_s}{\Sigma_t} = \mathrm{Re}[W_j]\frac{\Sigma_s}{\Sigma_t} + i \cdot \mathrm{Im}[W_j]\frac{\Sigma_s}{\Sigma_t}, \tag{9}$$

after the collision, where Re[·] = real part and Im[·] = imaginary part. The Russian roulette game is applied separately to the real and imaginary parts when either or both of $\left|\mathrm{Re}[W_j']\right|$ and $\left|\mathrm{Im}[W_j']\right|$ are less than a lower weight cutoff boundary. When either the real or imaginary part is killed but the other part still survives, the particle keeps being transported. The particle with the complex-valued weight is killed by the Russian roulette game only when both its real and imaginary parts are killed at the same time.

(3) Treatment of fission neutrons

The determination of the reaction type at each collision is identical to that of the conventional Monte Carlo method. As seen in Eq. (4), however, the weight of each particle produced by a fission reaction is given by

$$W_{jF} = \frac{W_j}{k_{eff}}\left(1 - \frac{i\omega\beta}{i\omega + \lambda}\right), \tag{10}$$

where W_j is a particle weight before weight reduction via implicit capture. The weight, W_{jF}, is assigned to each particle produced by the fission reaction.

A very similar algorithm was successfully implemented into the MCNP code for adding a new function of the B_1 approximation (Yamamoto, 2012). The modified MCNP code was verified through comparison with other deterministic codes. In this paper, the algorithm shown above is also implemented into MCNP. In the next section, the modified MCNP is applied to neutron noise calculations in a one-dimensional homogeneous multiplying system. For verification of the modified code, the results are compared with those calculated using the 2-group in-house research-purpose Monte

Carlo code developed in (Yamamoto, 2013).

4. Numerical Tests using Monte Carlo Calculations for Neutron Noise Analyses

4.1. Verification through comparison with the 2-group calculations

In this section, a continuous energy Monte Carlo code modified for frequency domain calculations is used to calculate neutron noise distributions in an infinitely long cylindrical geometry. The cylinder is composed of a homogeneous uranyl nitrate aqueous solution. The ^{235}U enrichment is 9.98 wt%, and the uranium concentration is 254 g/L. For verification of the modified continuous energy Monte Carlo code, MCNP, two-energy group Monte Carlo calculations are performed as reference calculations using an in-house research-purpose code that was developed in (Yamamoto, 2013). The code for the reference calculations was verified through comparison with the deterministic calculations using diffusion theory (Yamamoto, 2013). The group constants used for the two-energy group calculations are prepared using the thermal reactor analysis code, SRAC (Okumura *et al.*, 2007). The energy boundary is 0.993 eV. The group constants are listed in Table 1. The anisotropic scattering is considered up to P_1 order. The cylinder has a diameter of 53.36 cm. A vacuum (i.e., non-reentrant) boundary condition is imposed at the outer boundary. An isotropic noise source is placed at the center of the cylinder. Source particles with a weight of unity are emitted only in the 2nd energy group (below 0.993 eV in the MCNP calculations). The multigroup and pointwise nuclear libraries used in this paper are based on the nuclear data library JENDL-4 (Shibata et al., 2011). The parameters of the delayed neutrons are $\beta = 0.007$ and $\lambda = 0.08$ s. Although the continuous energy Monte Carlo code can use the 6-group delayed neutron parameters (fraction, decay constant, and neutron spectrum) of each nuclide, this function is disabled in the modified code in this work.

[Table 1]

Before performing the neutron noise calculations, the criticality calculations for k_{eff}'s used in Eq. (4) are performed using MCNP and the multigroup code. The k_{eff}'s are 0.99996 ± 0.00008 and 0.93292 ± 0.00007, respectively. The difference between the calculated k_{eff}s is relatively large, which is understandable considering the group condensation, the scattering treatment, and some other approximations in the two-energy group calculation. The comparison between the two Monte Carlo calculation codes is not meant to achieve complete agreement between them. The objective of the comparison is to determine whether the neutron noise calculations using the continuous energy Monte Carlo code can reproduce the tendency of the multigroup calculations.

The continuous energy Monte Carlo calculations, which are incapable of suppressing the diverging particle population, can be performed for the frequency range between 0.02 Hz and 15 Hz. The prompt neutron generation time of the fuel solution is 64.2 ± 0.3 μs, which is calculated using MCNP6 (Pelowitz et al., 2014) based on an option for the point-kinetics parameters (the iterated fission probability method). Thus, the plateau frequency range is roughly from 0.01 Hz (= $\lambda/(2\pi)$) to 17 Hz (= $(\lambda + \beta/\Lambda)/(2\pi)$). This range is almost identical to the frequency range (0.02 Hz ~ 15 Hz) in which the continuous energy Monte Carlo calculations for the neutron noise in the fuel solution can be performed. Figs. 1 and 2 show the radial distributions of the real part and the imaginary part of the neutron noise in the 1st group, respectively. The neutron noise flux is calculated using the track length estimator. In the figures, the results calculated using MCNP are compared with those using the two-energy group code for the frequency of 0.02 Hz as a representative of many results. Each neutron noise flux is normalized to be the same at the innermost point. Figs. 3 and 4 show the same results

for the 2nd group. Although the results calculated using the MCNP code do not necessarily agree well with those obtained using the two-energy group code, the qualitative trends of the noise distributions are well reproduced. The trend for 0.02 Hz shown in Figs. 1-4 can be observed at other frequencies between 0.02 Hz and 15 Hz. The phase shifts and the amplitudes of the neutron noise in the 2nd group calculated using both codes are compared in Figs. 5 and 6, respectively. The position of the neutron noise is located at r = 13.34 cm (the midpoint between the center of the cylinder and the outer boundary). The amplitude of each neutron noise signal is normalized to be the same at 1 Hz. In the same manner as the flux distributions, the phase shifts and the amplitudes calculated using MCNP are in qualitative agreement with those using the two-energy group code. In conclusion, the Monte Carlo algorithm for solving the neutron noise equation in the frequency domain has been successfully implemented into a production-level continuous energy Monte Carlo code insofar as the frequency is within the range of the plateau frequency.

[Fig. 1][Fig. 2][Fig. 3][Fig. 4][Fig. 5][Fig. 6]

4.2. Neutron noise calculations in a BWR benchmark model

The MCNP code modified for neutron noise calculations is used for the analysis of the neutron noise propagation in the benchmark model of a BWR core. The geometry of the fuel assembly is based on the benchmark model proposed by the special committee of the Atomic Energy Society of Japan (2003). The geometry of the assembly and the materials of the fuel rods are shown in Fig. 7. Two water rods are installed in the assembly. The cladding and the channel box are made of zirconium. The void fraction is 0% in the water rods and the water channel. Within the channel box, three cases are considered for the void fraction: 0%, 40%, and 70%. The whole core of this model is composed of a 16 by 16 array of the unirradiated assemblies, as shown in Fig. 8. All

fuel assemblies are identical, and they extend infinitely and uniformly in the vertical direction. No control rod is included in this model. The temperatures of the fuel pellets and other materials are 900 K and 600 K, respectively. This model does not represent a realistic core configuration. The objective of this study is not to perform a faithful noise simulation in a BWR in operation; rather, the objective is to investigate the property of noise propagation in an array of BWR assemblies.

[Fig. 7][Fig. 8]

An isotropic point noise source is placed at the center of the core, as shown in Fig. 9, which is a magnified figure of the area enclosed by the dotted square in Fig. 8. The noise source point is located at the intersection of the water channel. The energy spectrum of the noise source is assumed to be the same as the thermal neutron spectrum at the source position. The spectrum of the noise source is shown in Fig. 10. The noise source is emitted below 1 eV. Thus, the noise source is given by

$$S(\mathbf{r},\mathbf{\Omega},E,\omega) \propto \begin{cases} \int_{4\pi} \phi_0(\mathbf{r},\mathbf{\Omega},E)d\mathbf{\Omega}, & E \le 1eV \\ 0, & E > 1eV, \end{cases} \tag{11}$$

where $\phi_0(\mathbf{r},\mathbf{\Omega},E)$ is calculated in the k_{eff}-eigenvalue calculation for the model. The neutron noise is detected at the intersections of the water channels where the in-core monitors are installed in a BWR. The detection positions are shown in Fig. 9. An empty cylinder with a height of 10 cm and a diameter of 1.76 cm is placed at each detector position at the same elevation as the noise source. A particle with a complex-valued weight passing through the empty cylinder is tallied as a noise signal using the track length estimator.

[Fig. 9][Fig. 10]

The criticality calculations are performed to obtain the value of k_{eff} that is used in Eq. (10). The k_{eff}'s for the core with the void fraction of 0%, 40%, and 70% are 1.08934

± 0.00010, 1.05973 ± 0.00009, and 1.02631 ± 0.00010, respectively. The prompt neutron generation times that are calculated using MCNP6 are 26.2 ± 0.2 μs, 25.7 ± 0.2 μs, and 25.2 ± 0.2 μs for the void fractions of 0%, 40%, and 70%, respectively. Therefore, the plateau frequency range is from approximately 0.01 Hz to 44 Hz. Alternatively, the frequency range where the neutron noise calculations can be successfully performed using MCNP ranges from 0.02 Hz to 35 Hz.

Fig. 11 shows the horizontal distribution of the amplitude of the thermal neutron noise (below 1 eV) for several frequencies (0.02 Hz, 1 Hz, and 35 Hz). The void fraction in Fig. 11 is 40%. The amplitude naturally decays with the distance from the noise source. Fig. 12 shows the horizontal distribution of the amplitude of the thermal neutron noise at 1 Hz for the void fractions of 0%, 40%, and 70%. Each amplitude is normalized to be the same at the nearest detector position. The neutron noise decays more rapidly with the distance from the noise source as the void fraction decreases because the neutron noise is prone to undergo more scattering and absorption in a lower void fraction. This can be easily deduced by analogy with the propagation of neutrons.

[Fig. 11][Fig. 12]

The frequency dependence of the amplitude of the thermal neutron noise for the void fraction of 40% is shown in Fig. 13. The frequency dependences at two positions ("H1" and "D3" in Fig. 9) are compared. The frequency dependence of the point kinetics approximation is also shown in Fig. 13. Under the point kinetics approximation, the frequency dependence of the neutron noise is represented by the zero-power reactor transfer function (Duderstadt and Hamilton, 1976):

$$G_0(\omega) = \frac{1}{i\omega\left(\Lambda + \frac{\beta}{\lambda + i\omega}\right)}, \tag{12}$$

where Λ = 25.7 μs, β = 0.007, and λ = 0.08 s^{-1}. As seen in Fig. 13, the frequency

dependence of the thermal neutron noise is relatively small at the position near the noise source, “H1”, and the dependence becomes more significant with the distance from the noise source. At position “D3”, which is 65 cm away from the noise source, the frequency dependence is close to that of the point kinetics. Fig. 14 compares the phase shift of the thermal neutron noise at several detector positions (“H1”, “H2”, “H3”, and “H4”). The phase shift of the point kinetics $G_0(\omega)$ is also shown in Fig. 14. In the same manner as the amplitude, the phase shift varies slightly with the frequency at the position near the noise source (“H1”), and it differs greatly from the point kinetics. In contrast, as the detector position departs from the noise source, the phase shift approaches the point kinetics behavior.

[Fig. 13][Fig. 14]

These spatial dependences and the departure from the point kinetics behavior can be explained by considering that the neutron noise comprises higher order modes. Although the quantitative investigation of the higher mode effects is an important subject for the reactor noise research, this subject is beyond the scope of this paper and will be considered in future work. A recent approach to investigate the space-dependence of the neutron noise proposed by Pázsit and Dykin (2018) may be promising. We can conclude that the frequency dependence of the neutron noise is largely affected by the detector position. Although the detector near the noise source is very sensitive to the noise source, the detected neutron noise may deviate from the point kinetics behavior. This characteristic regarding the spatial dependence of the neutron noise must be considered when we conduct neutron noise research.

The efficiency of the neutron noise calculation depends on the frequency. As the frequency decreases toward zero, the neutron noise equation, Eq. (4), becomes equivalent to the fixed source calculation in a critical state, where the fission chain

reactions continue endlessly. Alternatively, in the high frequency region, an unmanageable number of particles are produced via the third term on the right-hand side of Eq. (4) (i.e., $-i\omega\delta\phi/\upsilon$). Thus, the calculation efficiency becomes worse in the low- and high-frequency ranges. Fig. 15 shows the relative figure of merit of the amplitude of the thermal neutron noise at position "H1" as a function of frequency. The calculation efficiency is maximum at approximately 1 Hz. The current Monte Carlo algorithm used in this study is not only inapplicable to the frequency outside the plateau range but also requires a long calculation time for the frequency range, even if the calculation can be successfully performed. The future work involves developing a novel algorithm to streamline the noise calculation to reduce the calculation time as well as preventing the exploding number of particles in the low and high frequencies.

[Fig. 15]

5. Conclusions

The Monte Carlo algorithm for solving the neutron noise equation in the frequency domain was implemented into a production-level continuous energy Monte Carlo code. One of the difficulties in the Monte Carlo algorithm is determining how to control the growing number of particles produced for the low- or high-frequency noise. Some techniques have been proposed in (Yamamoto, 2013) and (Rouchon et al., 2017) to circumvent this difficulty. However, implementing these techniques into the modified code would require major modifications and was thus not considered in this study. The modified code can be applicable to the approximate frequency range between 0.02 Hz and $\lambda + \beta/\Lambda$ (several tens of Hz). The modified MCNP code was used for the neutron noise calculations in a one-dimensional homogeneous fuel solution. The calculation results are compared with those obtained using the two-energy group in-house research-purpose code. The relatively good agreement between the two codes pointed

out the validity of the modified MCNP code.

The modified MCNP code is applied to the neutron noise calculations for a collection of benchmark model BWR assemblies. Near the neutron noise source, the frequency dependence of the amplitude and the phase shift differs largely from that of the point kinetics. However, the frequency dependence becomes similar to the point kinetics as the detector departs from the noise source. Such a spatial dependence of the neutron noise is considered to be caused by higher mode effects. The neutron noise detected near the noise source is most sensitive to the neutron source, and it is likely to deviate from the point kinetics behavior. The higher order mode effect must be considered as one of the targets of future work.

The implementation of the algorithm for controlling the number of particles remains a topic for future work. The weight cancellation method (Yamamoto, 2013) is difficult to implement into a production-level Monte Carlo code. The method proposed by Rouchon et al. (2017), where the implicit capture is disabled and a pseudo total cross section is added to the noise equation, is expected to be viable in a production-level Monte Carlo code. However, the calculation efficiency becomes worse outside the plateau frequency range. Thus, a novel algorithm for improving the calculation efficiency should be pursued for future development of this research.

Acknowledgement

The present research project was supported by JSPS KAKENHI Grant Number JP17K07011. This work was prompted by the author's involvement in the CORTEX project. The author wishes to acknowledge the member of the CORTEX project for their comments and suggestions.

References

Atomic Energy Society of Japan, 2003. Benchmark models for Monte Carlo calculations, available on CD-ROM (in Japanese).

Behringer, K., Kosály, G., Kostić, L., 1977. Theoretical investigation of the local and global components of the neutron-noise field in a boiling water reactor. Nucl. Sci. Eng., 63, 306-318.

Behringer, K., Kosály, G., Pázsit, I., 1979. Linear response of the neutron field to a propagating perturbation of moderator density (two-group theory of boiling water reactor noise). Nucl. Sci. Eng., 72, 304-321.

Briesmeister, J.F., Ed. 2000. MCNP—A General Monte Carlo N-particle transport code, version 4C. LA-13709-M.

Demazière, C., Andhill, G., 2005. Identification and localization of absorbers of variable strength in nuclear reactors. Ann. Nucl. Energy, 32, 812-842.

Demazière, C., 2004. Development of a 2-D 2-group neutron noise simulator. Ann. Nucl. Energy, 31, 647-680.

Demazière, C., 2011. CORE SIM: A multi-purpose neutronic tool for research and education. Ann. Nucl. Energy, 38, 2698-2718.

Demazière, C., Pázsit, I., 2009. Numerical tools applied to power reactor analysis. Prog. Nucl. Energy 51, 67-81.

Demazière, C., Vinai, P., Hursin, M., Kollias, S., Herb, J., 2017. Noise-based core monitoring and diagnostics—Overview of the CORTEX project. Proc. Advances in Reactor Physics (ARP-2017), Mumbai, India, December 6-9, 2017.

Duderstadt, J.J., Hamilton, L.J., 1976. Nuclear Reactor Analysis. John Wiley & Sons.

Glöckler, O., Pázsit, I., 1987. Spatial noise-source reconstruction. Ann. Nucl. Energy 14,

63-75.

Hosseini, S.A., Vosoughi, N., 2012. Neutron noise simulation by GFEM and unstructured triangle elements. Nucl., Eng. Design 253, 238-258.

Hosseini, S.A., Vosoughi, N., 2013. On a various noise source reconstruction algorithms in VVER-1000 reactor core. Nucl. Eng. Design 261, 132-143.

Hosseini, S.A., Vosoughi, N., 2014. Noise source reconstruction using ANN and hybrid methods in VVER-1000 reactor core. Prog. Nucl. Energy 71, 232-247.

Jonsson, A., Tran, H.N., Dykin, V., Pázsit, I., 2012. Analytical investigation of the properties of the neutron noise induced by vibrating absorber and fuel rods. Kerntechnik 77, 371-380.

Larsson, V., Demazière, C., Pázsit, I., Tran, H.N., 2011. Neutron noise calculations using the Analytical Nodal Method and comparisons with analytical solutions. Ann. Nucl. Energy, 38, 808-816.

Larsson, V., Demazière, C., 2012a. A coupled neutronics/thermal-hydraulics tool for calculating fluctuations in Pressurized Water Reactors. Ann. Nucl. Energy, 43, 68-76.

Larsson, V., Demazière, C., 2012b. Comparison of the calculated neutron noise using finite differences and the Analytical Nodal Method. Ann. Nucl. Energy, 43, 176-182.

Okumura, K., Kugo, T., Kaneno, K., Tsuchihashi, K., 2007. SRAC2006: A comprehensive neutronics calculation code system, JAEA-Data/Code 2007-004.

Pázsit, I., Analytis, G. TH., 1980. Theoretical investigation of the neutron noise diagnostics of two-dimensional control rod vibrations in a PWR. Ann. Nucl. Energy 7, 171-183.

Pázsit, I., Demazière, C., 2010. Noise techniques in nuclear systems. In: Cacuci, D.G., Ed., Handbook of Nuclear Engineering, Vol.3, 1629-1737, Springer.

Pázsit, I., Dykin, V., 2018. The role of the eigenvalue separation in reactor dynamics and neutron noise theory. J. Nucl. Sci. Technol. (in press).

Pelowitz, D., Fallgren, A.J., McMath, G.E., Ed., 2014. MCNP6™ user's manual code version 6.1.1 beta, LA-CP-14-00745.

Rouchon, A., Zoia, A., Sanchez, R., 2017. A new Monte Carlo method for neutron noise calculations in the frequency domain. Ann. Nucl. Energy, 102, 465-475.

Shibata, K., Iwamoto, O., Nakagawa, T., Iwamoto, N., Ichihara, A., Kunieda, S., Chiba, S., Furutaka, K., Otuka, N., Ohsawa, T., Murata, T., Matsunobu, H., Zukeran, A., Kamada, S., Katakura, J., 2011. JENDL-4.0: A new library for nuclear science and engineering, J. Nucl. Sci. Technol., 48(1), 1-30.

Viebach, M., Bernt, N., Lange C., Hennig, D., Hurtado, A., 2017. On the influence of dynamical fuel assembly deflections on the neutron noise level. Prog. Nucl. Energy (in press).

Yamamoto, T., 2012. Monte Carlo method with complex weights for neutron leakage-corrected calculations and anisotropic diffusion coefficient generations. Ann. Nucl. Energy, 50, 141-149.

Yamamoto, T., 2013. Monte Carlo method with complex-valued weights for frequency domain analyses of neutron noise. Ann. Nucl. Energy 58, 72-79.

Yamamoto, T., Sakamoto, H., 2015. Dynamic Monte Carlo calculation method by solving frequency domain transport equation using the complex-valued weight Monte Carlo method. Ann. Nucl. Energy 85, 426-433.

Figure legend

Fig. 1 Distribution of neutron noise in the 1st group (real part).

Fig. 2 Distribution of neutron noise in the 1st group (imaginary part).

Fig. 3 Distribution of neutron noise in the 2nd group (real part).

Fig. 4 Distribution of neutron noise in the 2nd group (imaginary part).

Fig. 5 Amplitude of neutron noise in the 2nd group vs. frequency.

Fig. 6 Phase shift of neutron noise in the 2nd group vs. frequency.

Fig. 7 BWR assembly for neutron noise calculations.

Fig. 8 Plan view of the entire core configuration for the noise calculations.

Fig. 9 Magnified figure of the area enclosed by the dotted square in Fig. 8.

Fig. 10 Spectrum of the noise source.

Fig. 11 Horizontal distribution of thermal neutron noise (40% void fraction).

Fig. 12 Horizontal distribution of thermal neutron noise (1 Hz).

Fig. 13 Amplitude of thermal neutron noise near and far from the noise source and point kinetics vs. frequency.

Fig. 14 Phase shift of thermal neutron noise at several points and point kinetics vs. frequency.

Fig. 15 Relative figure of merit of amplitude vs. frequency at “H1”.

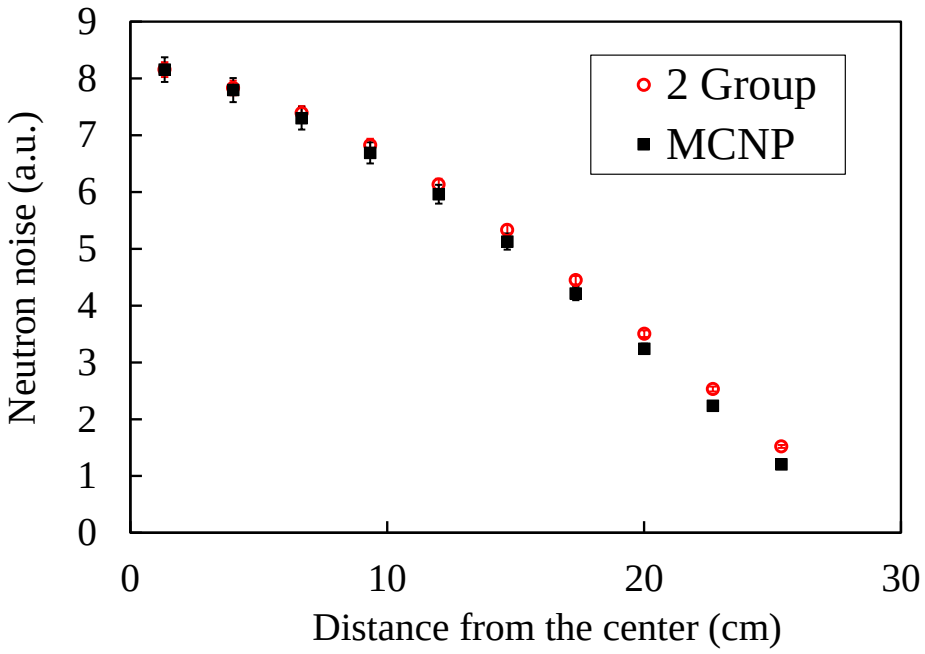

Fig. 1 Distribution of neutron noise in the 1st group (real part).

Yamamoto

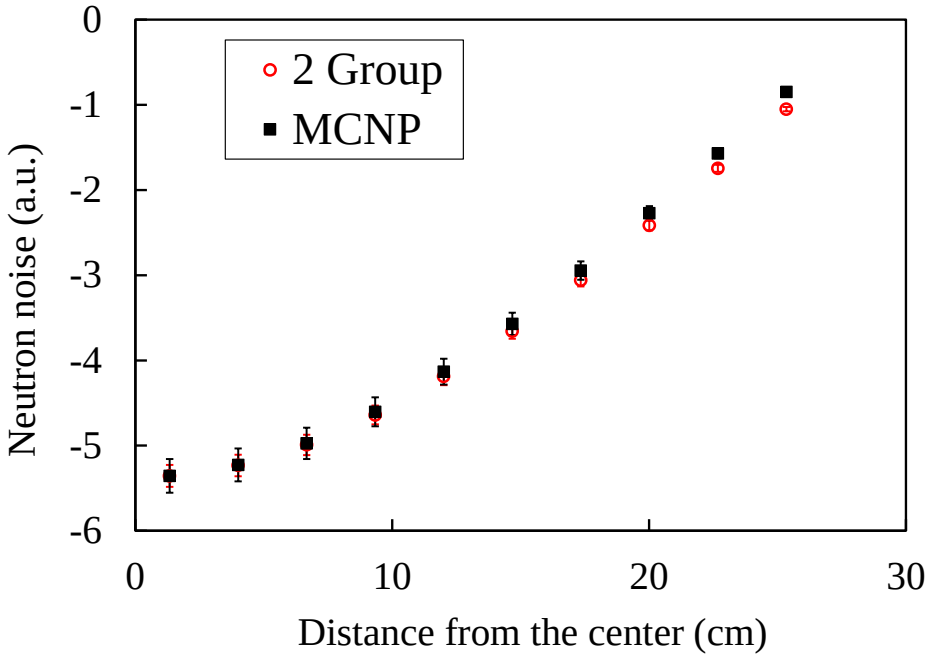

Fig. 2 Distribution of neutron noise in the 1st group (imaginary part).

Yamamoto

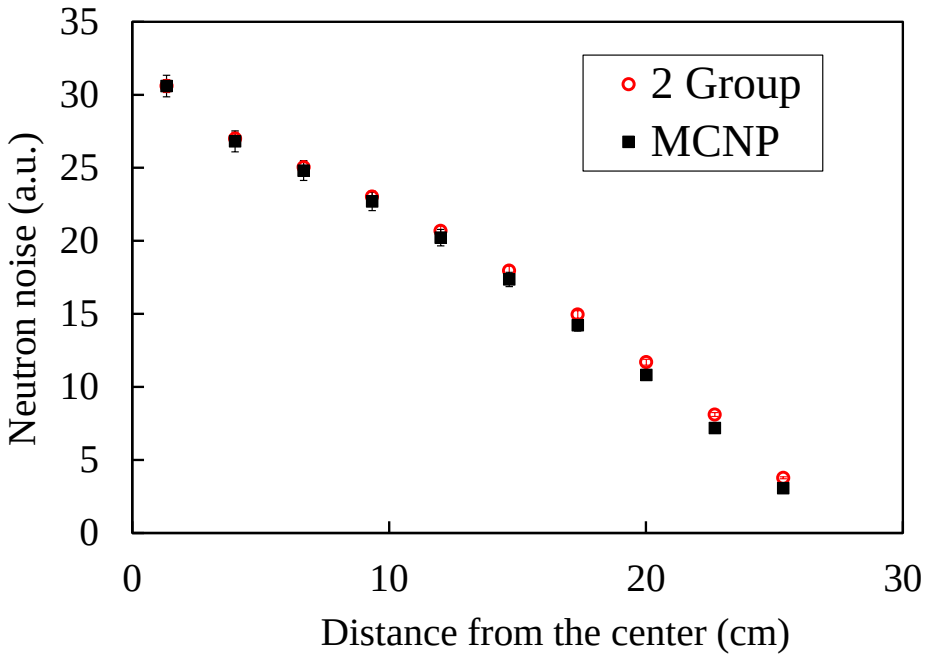

Fig. 3 Distribution of neutron noise in the 2nd group (real part).

Yamamoto

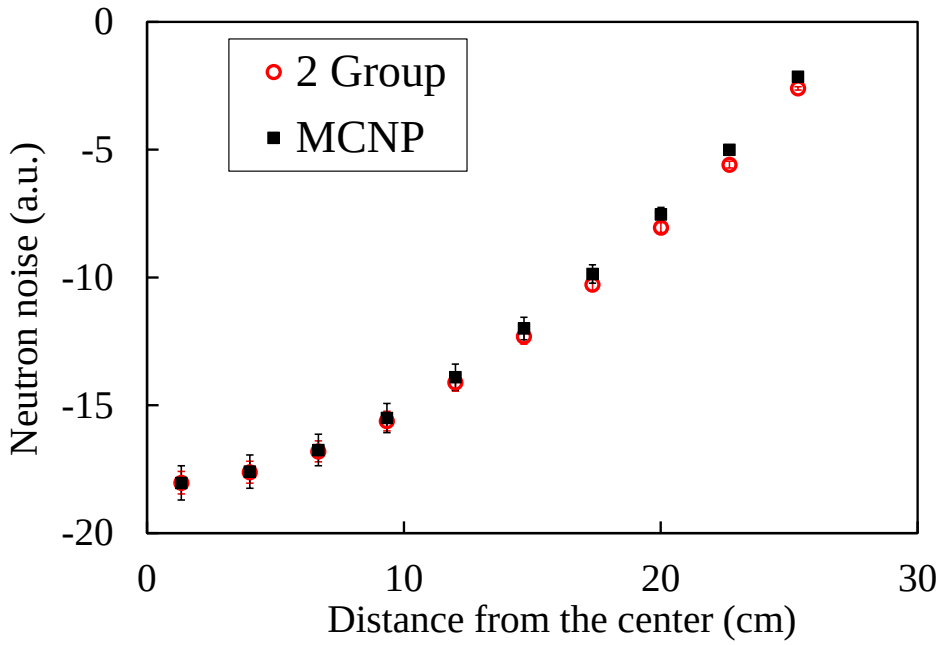

Fig. 4 Distribution of neutron noise in the 2nd group (imaginary part).

Yamamoto

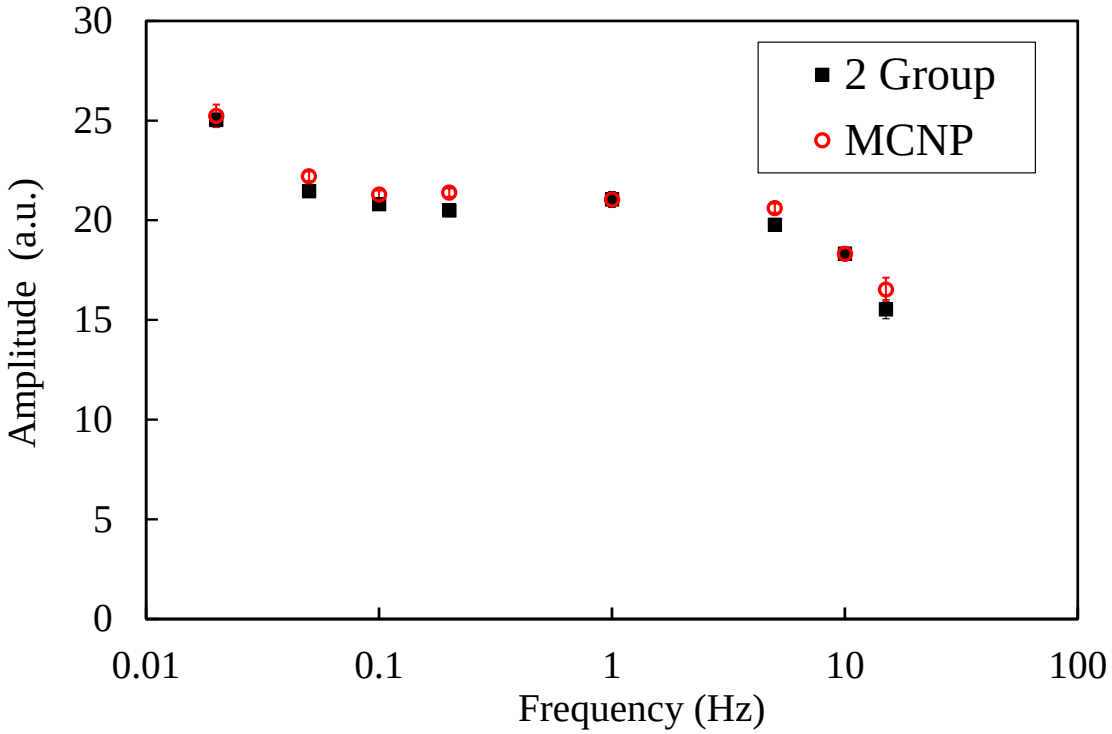

Fig. 5 Amplitude of neutron noise in the 2nd group vs. frequency.

Yamamoto

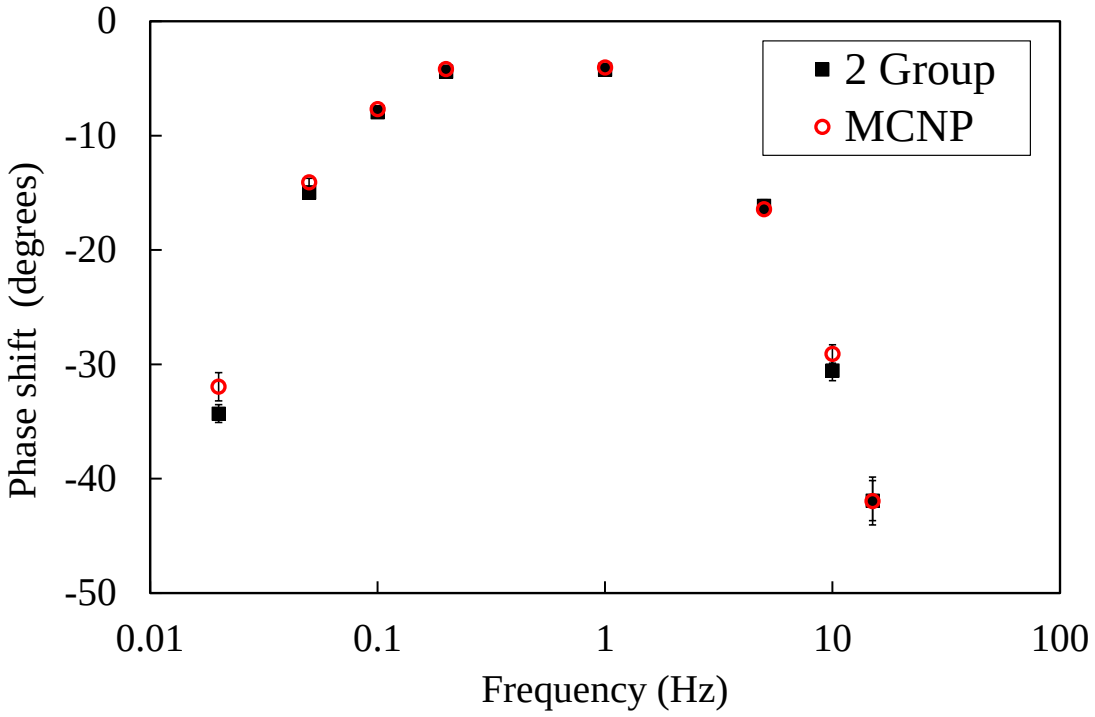

Fig. 6 Phase shift of neutron noise in the 2nd group vs. frequency.

Yamamoto

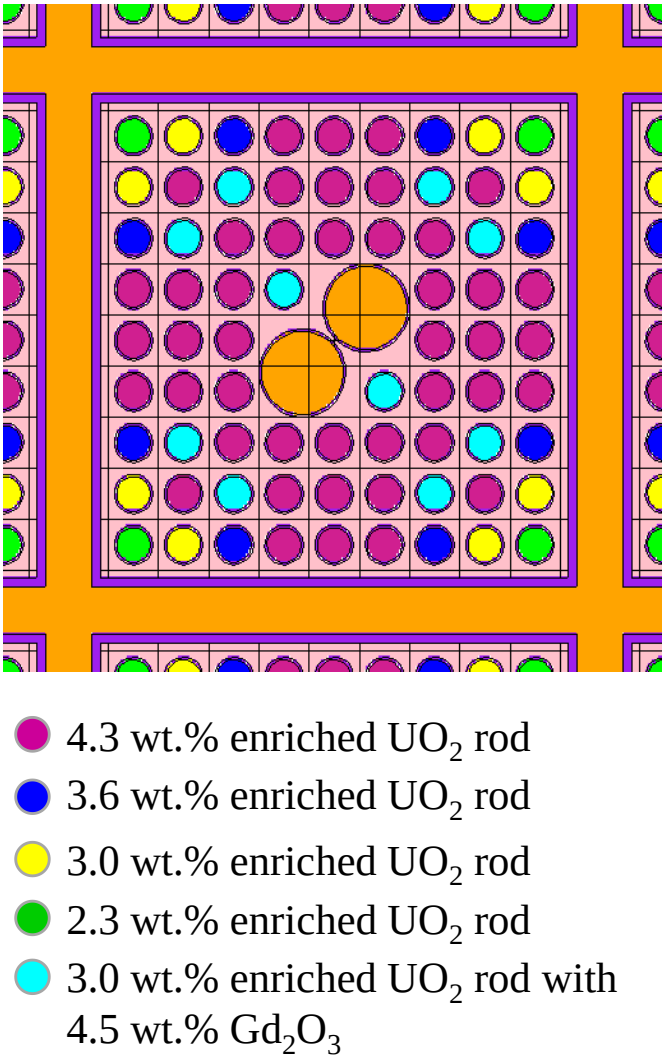

Fig. 7 BWR assembly for neutron noise calculations.

Yamamoto

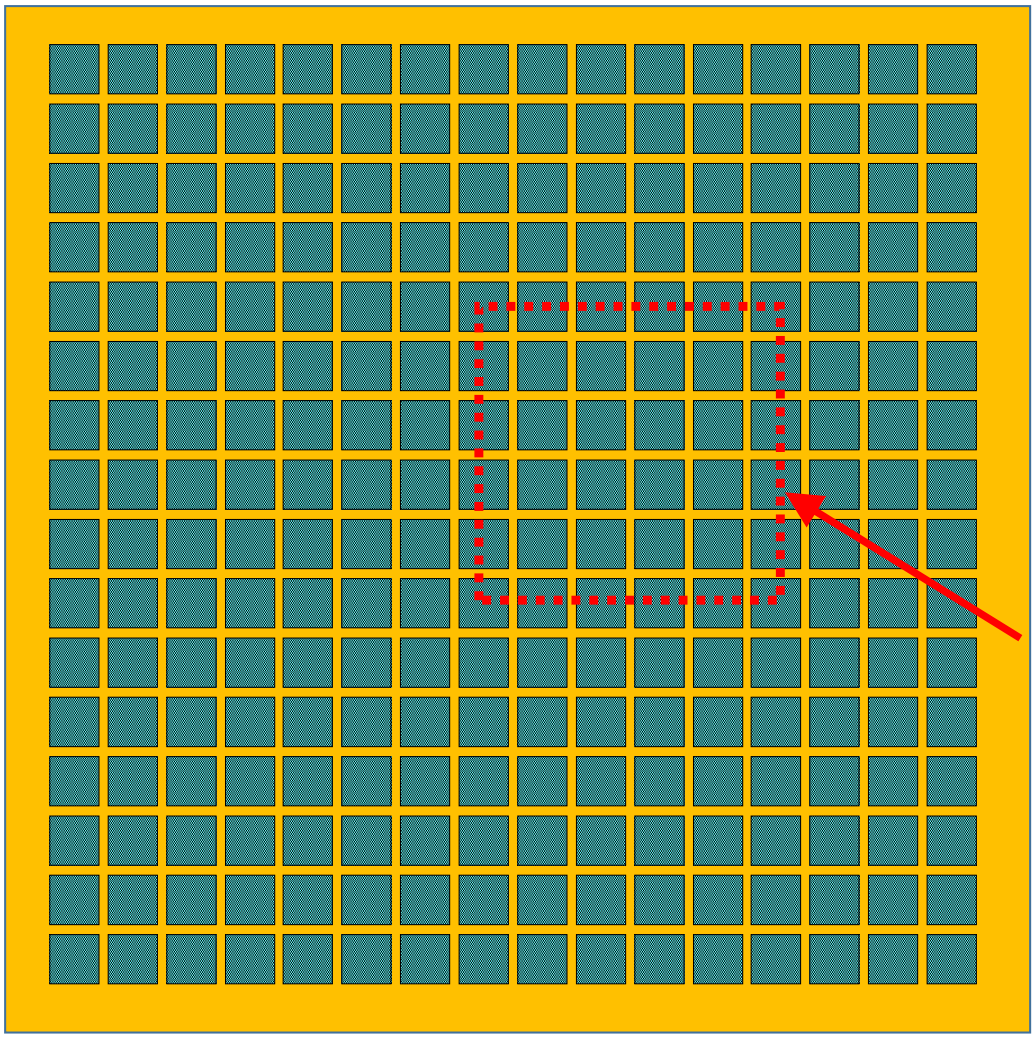

Fig. 9

Fig. 8 Plan view of the entire core configuration for the noise calculations.

Yamamoto

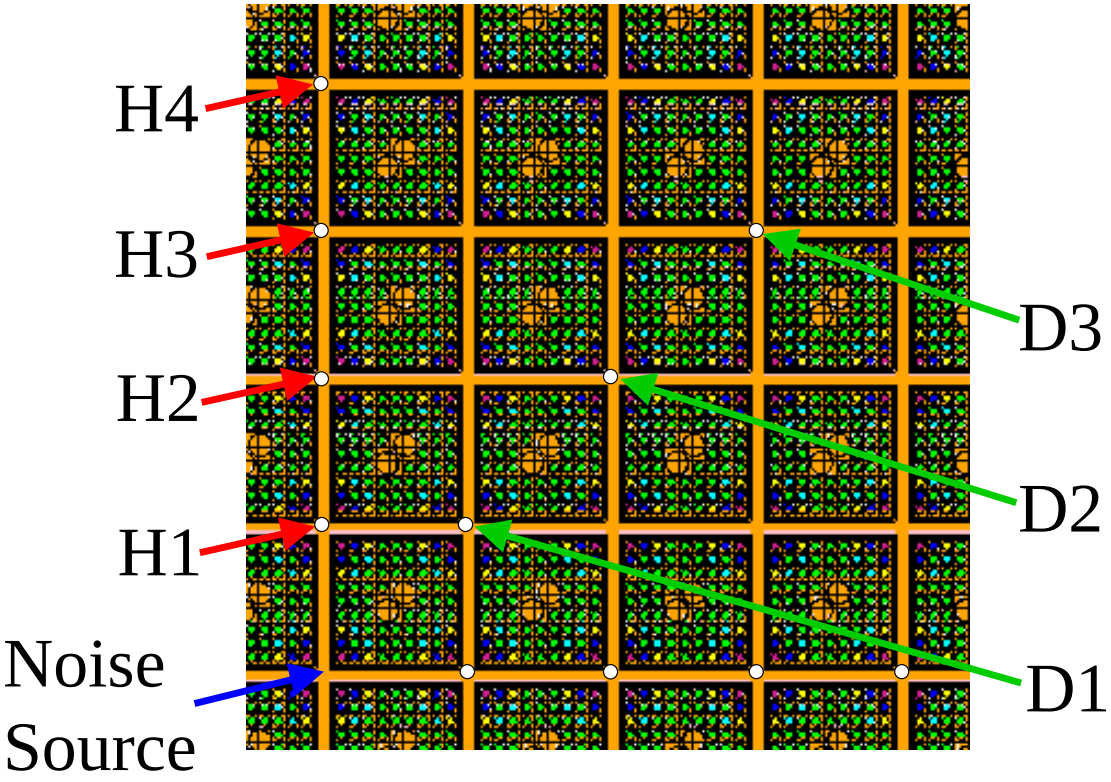

Fig. 9 Magnified figure of the area enclosed by the dotted square in Fig. 8.

Yamamoto

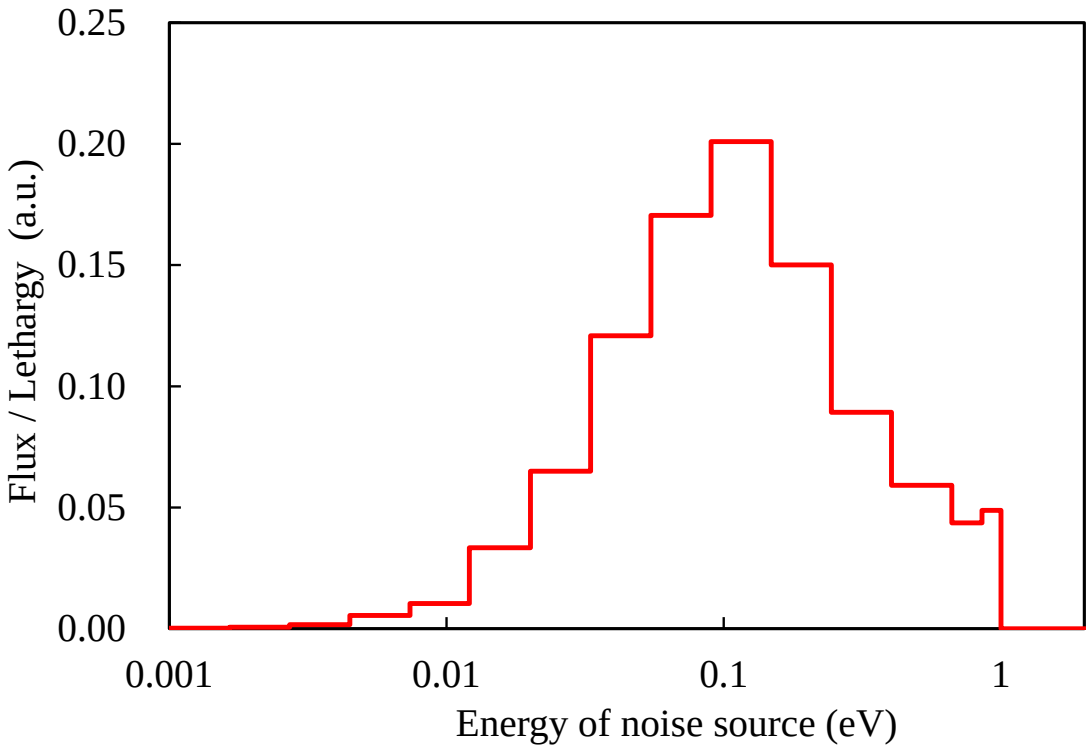

Fig. 10 Spectrum of the noise source.

Yamamoto

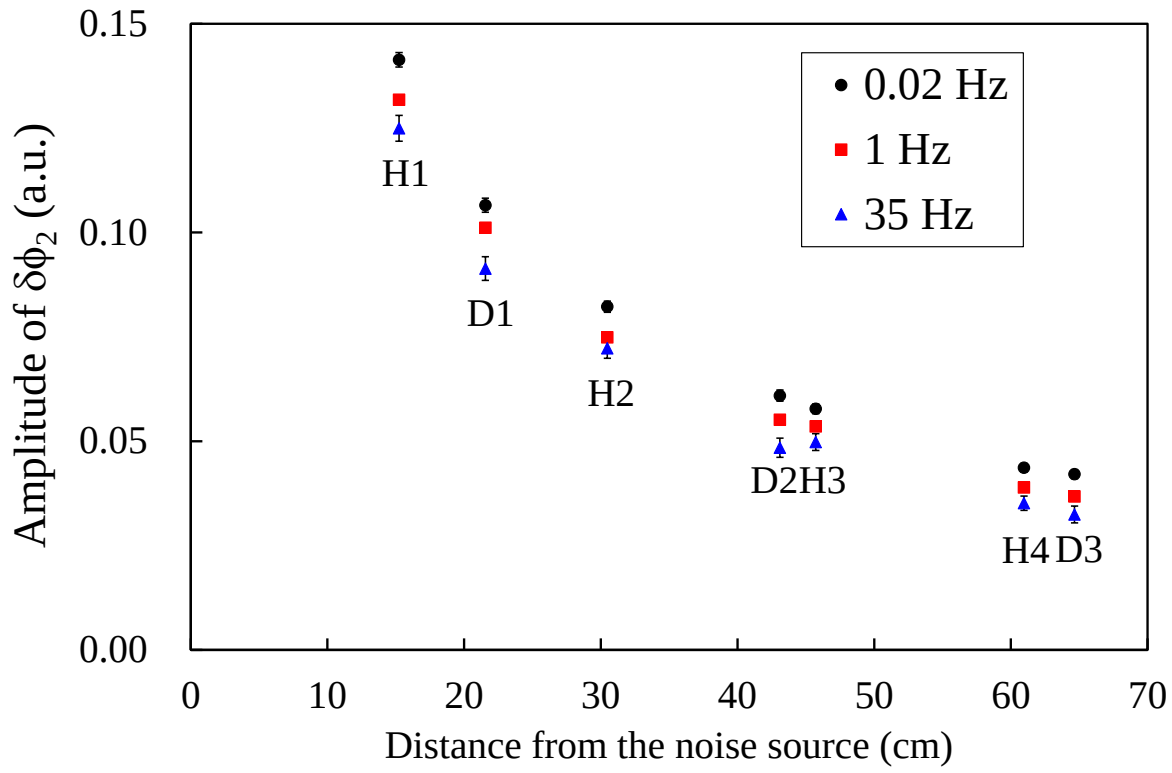

Fig. 11 Horizontal distribution of thermal neutron noise (40% void fraction).

Yamamoto

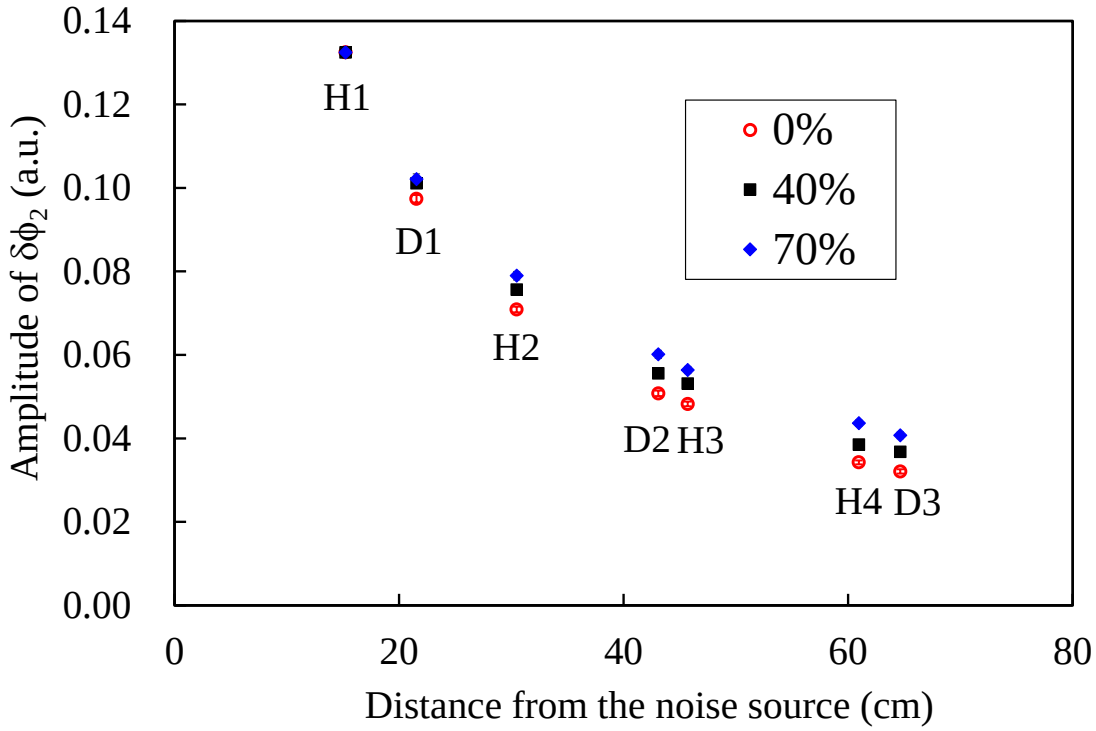

Fig. 12 Horizontal distribution of thermal neutron noise (1 Hz).

Yamamoto

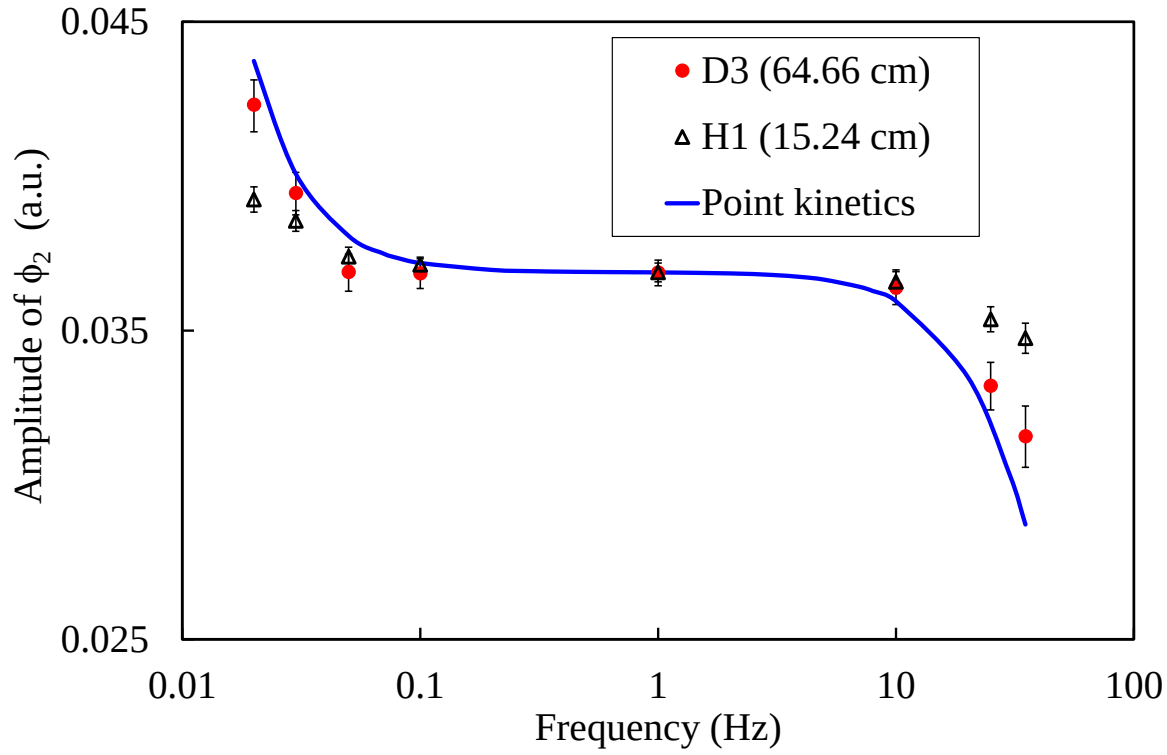

Fig. 13 Amplitude of thermal neutron noise near and far from the noise source and point kinetics vs. frequency.

Yamamoto

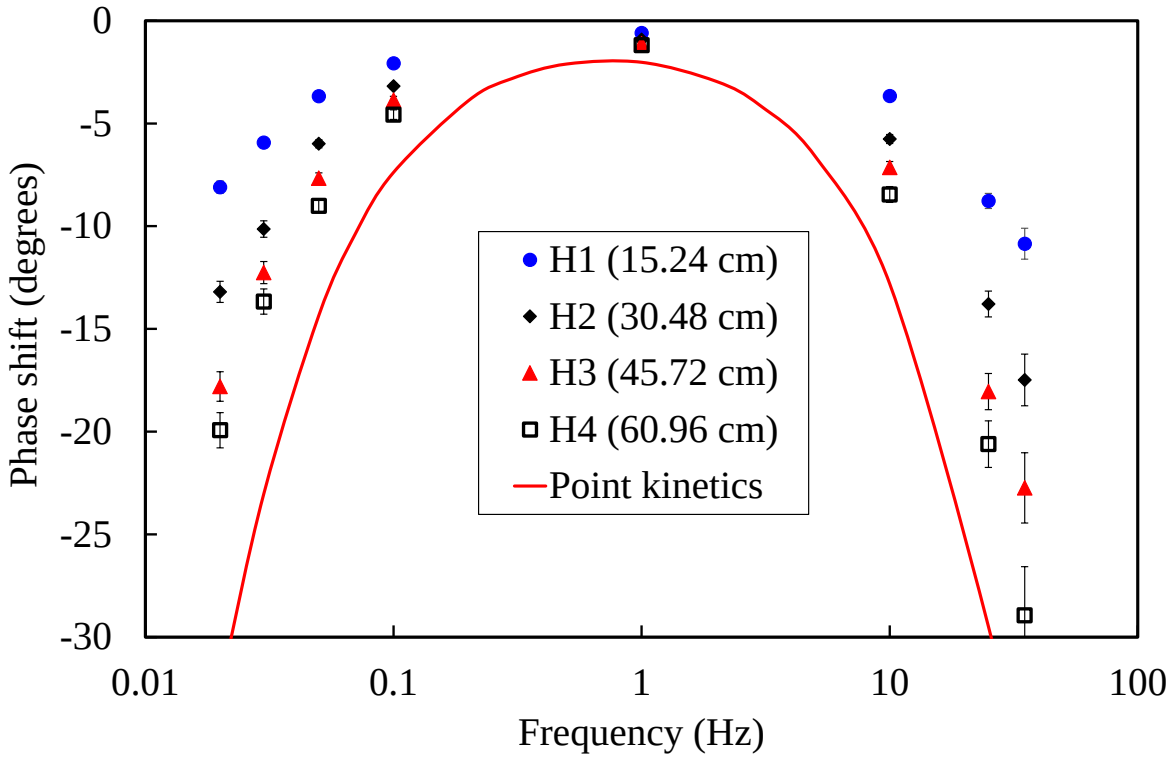

Fig. 14 Phase shift of thermal neutron noise at several points and point kinetics vs. frequency.

Yamamoto

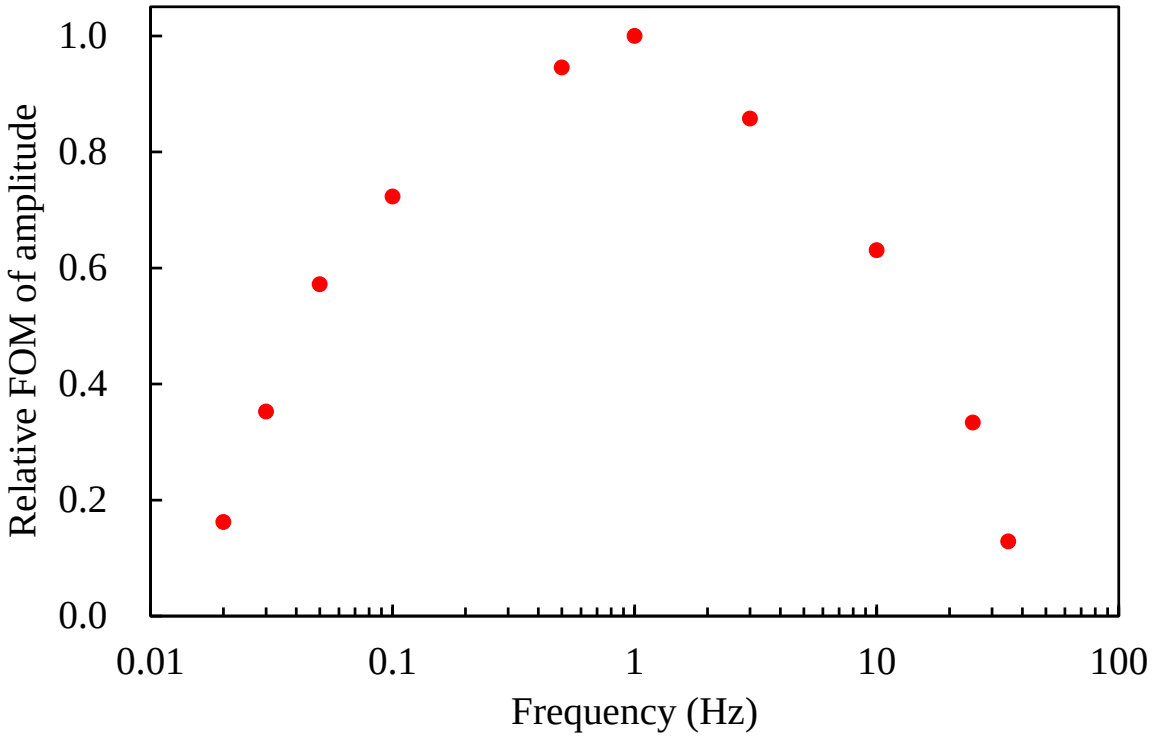

Fig. 15 Relative figure of merit of amplitude vs. frequency at “H1”.

Yamamoto

Table 1　2-group constants of uranium solution used for the neutron noise calculations.

	1st group (10 MeV ～ 0.993 eV)	2nd group (0.993 eV ～)
Σ_t (cm^{-1})	5.2521E-1*	2.4809E+0
Σ_c (cm^{-1})	3.1443E-3	2.4527E-2
$\nu\Sigma_f$ (cm^{-1})	1.5657E-3	6.9229E-2
$\Sigma_{s0g\to g}$ $(cm^{-1})^{**}$	4.8226E-1	2.4275E+0
$\Sigma_{s1g\to g}$ $(cm^{-1})^{***}$	5.0618E-1	9.6501E-1
$\Sigma_{s0g\to g+1}$ $(cm^{-1})^{**}$	3.9151E-2	–
$\Sigma_{s1g\to g+1}$ $(cm^{-1})^{***}$	8.8551E-3	–
υ (cm/s)	2.0889E+7	2.8386E+5

*Read as 5.2521×10^{-1}, **P_0 component, ***P_1 component